Analysis of a transonic cascade with wall-modeled LES based on DGSEM

B.F. Klose, E.J. Munoz Lopez, A. Hergt, J. Klinner, M. Bergmann, and C. Morsbach

1 Introduction

High-Reynolds number flows, which typically occur in turbomachinery applications, require sufficiently well-resolved boundary layer discretizations to accurately capture the small spatial and temporal scales of vortical flow within these turbulent regions. Large-eddy simulations (LES) have seen a growing popularity in modeling these complex flows and generating numerical references, despite being computationally expensive [1]. A remedy to the strict resolution requirements of *wall-resolved* LES (WRLES) is the use of wall functions to model the inner part of the turbulent boundary layer based on analytic or empirical wall laws. In this so-called *wall-modeled* LES (WMLES) approach, the boundary layer is no longer explicitly resolved and the wall-shear stress entering the viscous fluxes is computed from the velocity some distance away from the wall [2, 3]. Because the grid sizing in WMLES is not governed by the $y^+ \leq 1$ condition, this family of schemes allows for significantly larger elements near the wall, resulting in a reduction of the number of degrees of freedom and larger time-step sizes for a given CFL number. The WMLES thereby enables the simulation of large-scale turbomachinery configurations or operating points that are otherwise computationally too expensive.

Being computationally efficient, geometrically flexible, and numerically robust [4, 5], the discontinuous Galerkin spectral element method (DGSEM) is a popular choice among the family of high-order spectral methods for simulations of complex, compressible flows. While WMLES is already established in the finite volume community [3], applications based on spectral methods are scarce. Only recently,

B.F. Klose
Institute of Test and Simulation for Gas Turbines, German Aerospace Center (DLR), Am Technologiezentrum 5, 86159 Augsburg, Germany, e-mail: bjoern.klose@dlr.de

E.J. Munoz Lopez · A. Hergt · J. Klinner · M. Bergmann · C. Morsbach
Institute of Propulsion Technology, German Aerospace Center (DLR), Linder Höhe, Cologne 51147, Germany

Frere [6] presented results of the wall-modeled LES approach with the discontinuous Galerkin method and elaborated on guidelines based on the canonical channel flow.

In this work, we assess a WMLES strategy for DGSEM adopted from Frere [6] and present results for a periodic channel flow at $Re_\tau = 2003$ and a transonic compressor cascade at $Re_{\text{in}} = 1.4 \times 10^6$. For simplicity, the WMLES simulations are based on constant velocity sampling locations at the bottom of the second high-order element in accordance with [6]. The cascade is simulated using WRLES, underresolved WRLES (URLES), WMLES and a mixed boundary condition (zones of low-Reynolds and wall function) to evaluate the effect of the wall-model on the transitional boundary layer characteristics.

2 Numerical method

DLR's flow solver for turbomachinery applications TRACE is used for the discretization of the governing Navier-Stokes equations. A discontinuous Galerkin spectral element method (DGSEM) with nodal collocation, i.e. the solution and quadrature points are both taken to be the Legendre-Gauss-Lobatto nodes, is applied in this work and yields an efficient numerical scheme with diagonal mass matrix. Numerical errors arising from the non-linearity of the advective fluxes and the limited precision of integration are addressed by employing kinetic-energy or entropy conserving split-form approximations of the inviscid fluxes [7, 4]. All simulations are conducted with the implicit (no-model) LES approach, i.e. the dissipation is added implicitly via the numerical dissipation of the Riemann solver. The Bassy-Rebay-1 (BR1) scheme [8] is applied for the viscous part and an explicit third-order Runge-Kutta scheme is used for the integration in time. For more details on the scheme, we refer the interested reader to Bergmann [5, 9].

For transonic flow, the finite-volume (FV) subcell shock capturing approach by Hennemann [10] is applied to locally blend the high-order operator with a first-order FV scheme to reduce unphysical oscillations across the shock. We employ the feature-based indicator by Fernandez [11], which is a linear function of the product of a dilatation sensor and a Ducros vorticity sensor.

In the WMLES approach, the Dirichlet no-slip boundary condition (BC) at the wall is relaxed and the viscous flux at the wall-boundary is imposed in form of wall-shear stress τ_w calculated from an empirical wall function. We have implemented and tested the wall-model approach by Frere [6] and evaluate the velocity at the bottom of the second cell from the wall. The shear stress is computed from the friction velocity, which is based on the wall function by Reichardt [12] and obtained iteratively via a Newton-Raphson method at each time step.

3 Results

3.1 Turbulent channel flow

We validate the implementation of the wall function for WMLES with DGSEM on the periodic, turbulent channel flow at a Reynolds number of $\mathrm{Re}_\tau = 2003$. The flow is simulated in a box of dimensions $[2\pi\delta, 2\delta, \pi\delta]$ consisting of $20 \times 10 \times 10$ elements with periodic boundaries in x- and z- direction. A constant volume source term in x direction compensates for the viscous losses. The elements are clustered towards the no-slip walls at $y = [0, 2\delta]$ for URLES, but evenly spaced in case of WMLES (according to the setup by [6]). The element size in case of the WMLES is therefore such that the velocity sampling location (bottom of the second element from the wall) is located at 0.2δ in accordance with the recommendation by Larsson [2]. Polynomial orders of $N = (4,5,7)$ are tested for URLES and $N = (4,5)$ for WMLES.

Fig. 1 shows that URLES are not able to capture the wall-shear stress accurately and the friction velocity profiles substantially deviate from the reference DNS. Applying the wall function (WMLES) improves the results and the log-region is captured accurately despite having fewer points in the boundary layer and none within the viscous sublayer.

3.2 Transonic compressor cascade

We simulate the flow over a transonic compressor cascade aiming to match the experiments by Klinner [14] for the off-design operating point with $\mathrm{Ma}_{\mathrm{MP1}} = 1.05$, $\mathrm{Re}_{\mathrm{MP1}} = 1.4 \times 10^6$ and $\alpha_{\mathrm{MP1}} = 60.6°$, where MP1 refers to the 'measurement plane 1' located half a pitch upstream of the leading edge (LE). A non-reflecting inlet

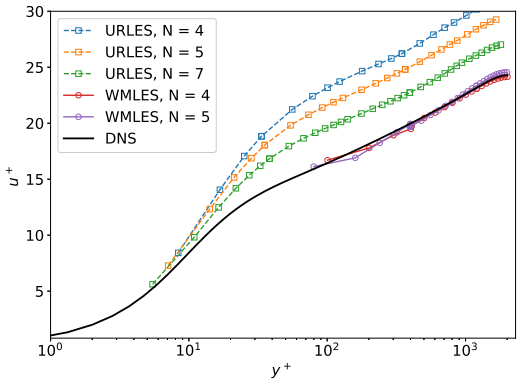

Fig. 1 Velocity profiles of URLES (dashed) and WMLES (solid) for the turbulent channel flow at $\mathrm{Re}_\tau = 2003$. The velocity sampling location is indicated by solid markers. The reference DNS by Hoyas & Jiminez [13] is given as solid, black line.

boundary [15] is located one pitch length upstream of the leading edge and a non-reflecting outlet boundary is applied 1.14 pitch lengths downstream from the trailing edge. The blade is extruded by 5% chord length along the span with periodic BCs applied in the spanwise, as well as the pitchwise direction. The entropy-conserving split-form variant by Chandrashekar [16] is used together with the corresponding Riemann solver and a uniform polynomial order of $N = 3$ (4th order accuracy in space) ensures that resolution jumps within the subcell-divided element are moderate.

Two meshes are employed in this study: the wall-refined grid G1 and the coarsened grid G2 whose first cell height corresponds to 0.2δ (δ = boundary layer thickness) measured at 10% of the absolute chord length c. Note that the streamwise element size of G2 is slightly lower than in G1 in order to follow the recommendation for elements with low aspect ratio for WMLES [6]. Three cases are compared: low-Reynolds wall treatment, wall-function treatment (with van-Driest compressibility correction) and a mixed BC, where the latter employs low-Reynolds treatment over the laminar section from the leading edge to the laminar separation bubble (LSB) and wall-function BC otherwise. An overview of the simulations in this work is given in Table 1:

Table 1 Overview of simulations.

Case	Wall BC	Grid	DOFs	Δt^*	y^+_{LE}	$\overline{y^+}$	t^*/CPUh
WRLES	LR	G1	145.7×10^6	7.0×10^{-6}	3.6	0.9	1.1×10^{-5}
URLES	LR	G2	132.8×10^6	1.8×10^{-5}	18.2	4.5	3.5×10^{-5}
Mixed	LR & WF	G2	132.8×10^6	1.8×10^{-5}	18.3	4.7	3.6×10^{-5}
WMLES	WF[a]	G2	132.8×10^6	1.8×10^{-5}	10.3	4.8	3.4×10^{-5}

LR = Low-Reynolds BC; WF = wall-function BC; DOF = degree of freedom; [a] = van-Driest corrected; $\overline{y^+} = \frac{1}{s}\int_0^s y^+(\hat{s})\mathrm{d}\hat{s}$; $t^* = t\cdot\overline{u}_0/c$; $\overline{u}_0$ = mean inflow velocity.

The surface isentropic Mach number, plotted in Fig. 2a, shows good agreement across all cases up to a near-constant offset to the experiments on the suction side. Only the case with wall-function treatment in the laminar region (WMLES) deviates from the reference WRLES and shows a less pronounced plateau upstream of the shock. The locally improved match with the experimental data is deemed coincidental, given that the deviation from the WRLES is increased. The discrepancy is associated with an over-prediction of the wall-shear stress in the laminar flow region upstream of the LSB, as seen in the skin friction coefficient C_f (Fig. 2b), and results in a delayed separation of the boundary layer and overall shortened bubble. Switching to wall-function BC within the LSB (mixed case) shows that the wall model under-predicts the transition peak in the shear stress and reattaches the flow slightly earlier than in the WRLES. Under-resolution (URLES), on the other hand, over-estimates the C_f peak but matches the reattachment point.

On the pressure side (PS), the boundary layer separates right at the LE and reattaches immediately within 5% of the chord. In the WRLES, spanwise vortices shed

from the bubble and gradually transition to turbulence on the pressure side. This shedding behavior is not captured by any of the cases on the coarser grid G2, which immediately transition to a fully turbulent boundary layer and yield a higher friction coefficient within the first 20% of the blade's chord length.

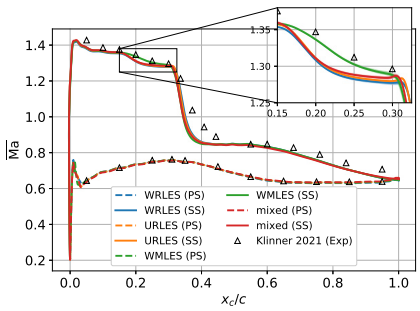

Fig. 2a Time- and span-averaged isentropic Mach number

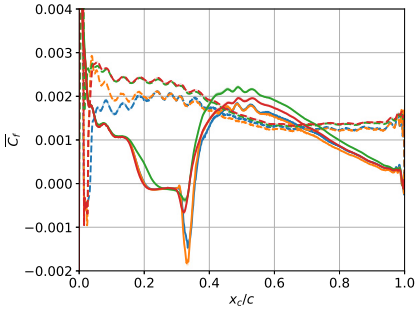

Fig. 2b Time- and span-averaged skin friction coefficient

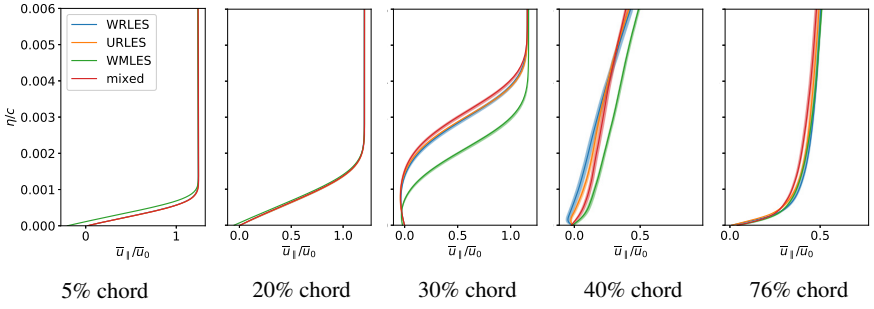

Fig. 3 Boundary layer profiles (normalized by the mean inflow velocity $\overline{u}_0$) on the suction side at various chord-wise locations.

The boundary layer shape is given for the different wall treatments at various locations in Fig. 3 and shows that all profiles, except for the case with full wall-function treatment (WMLES), collapse in the laminar flow region. The mismatch is caused by the over-estimation of the wall-shear stress at the LE because the velocity is probed too far away from the wall at the edge of the boundary layer, as the probing location is kept constant in this work. Within the separation bubble, the case with mixed BCs shows to have a slightly increased bubble height over the WRLES case, while delayed separation of the WMLES results in a significantly reduced bubble height. Downstream in the fully turbulent boundary layer, not surprisingly, all profiles converge again more closely. In all figures, the envelope of the curves indicates the 99% confidence interval of the averages.

4 Conclusion

We implemented and tested a simple wall function BC for DGSEM to be used for WMLES. The model is validated on the turbulent channel flow and shows that WMLES agrees well with reference DNS data, while under-resolved LES fails to correctly resolve the wall-shear stress when computed with the same number of degrees of freedom. Application of the model to a transonic compressor cascade emphasizes the challenging nature of such flows and shows that the wall function fails to accurately capture the laminar separation bubble and largely under-estimates the transition peak, while under-resolved low-Reynolds walls deliver results more closely matching WRLES. In the future, we plan to extend the WMLES approach to incorporate different models and a dynamic evaluation of the boundary layer to optimize the probe location and thereby improve the match with numerical reference data.

References

1. H. Choi and P. Moin, "Grid-point requirements for large eddy simulation: Chapman's estimates revisited," *Physics of Fluids*, vol. 24, p. 011702, jan 2012.
2. J. Larsson, S. Kawai, J. Bodart, and I. Bermejo-Moreno, "Large eddy simulation with modeled wall-stress: recent progress and future directions," *Mechanical Engineering Reviews*, vol. 3, no. 1, pp. 15–00418–15–00418, 2016.
3. S. T. Bose and G. I. Park, "Wall-modeled large-eddy simulation for complex turbulent flows," *Annual Review of Fluid Mechanics*, vol. 50, pp. 535–561, jan 2018.
4. A. R. Winters, R. C. Moura, G. Mengaldo, G. J. Gassner, S. Walch, J. Peiro, and S. J. Sherwin, "A comparative study on polynomial dealiasing and split form discontinuous galerkin schemes for under-resolved turbulence computations," *Journal of Computational Physics*, vol. 372, pp. 1–21, nov 2018.
5. M. Bergmann, C. Morsbach, and G. Ashcroft, "Assessment of split form nodal discontinuous galerkin schemes for the LES of a low pressure turbine profile," in *ERCOFTAC Series*, pp. 365–371, Springer International Publishing, 2020.
6. A. Frère, C. C. de Wiart, K. Hillewaert, P. Chatelain, and G. Winckelmans, "Application of wall-models to discontinuous galerkin LES," *Physics of Fluids*, vol. 29, p. 085111, aug 2017.
7. G. J. Gassner, A. R. Winters, and D. A. Kopriva, "Split form nodal discontinuous galerkin schemes with summation-by-parts property for the compressible euler equations," *Journal of Computational Physics*, vol. 327, pp. 39–66, dec 2016.
8. F. Bassi and S. Rebay, "A high-order accurate discontinuous finite element method for the numerical solution of the compressible navier–stokes equations," *Journal of Computational Physics*, vol. 131, pp. 267–279, mar 1997.
9. M. Bergmann, R. Gölden, and C. Morsbach, "Numerical investigation of split form nodal discontinuous galerkin schemes for the implicit les of a turbulent channel flow," in *Proceedings of the 7th European Conference on Computational Fluid Dynamics*, 2018.
10. S. Hennemann, A. M. Rueda-Ramírez, F. J. Hindenlang, and G. J. Gassner, "A provably entropy stable subcell shock capturing approach for high order split form DG for the compressible euler equations," *Journal of Computational Physics*, vol. 426, p. 109935, feb 2021.
11. P. Fernandez, N.-C. Nguyen, and J. Peraire, "A physics-based shock capturing method for large-eddy simulation," 2018.
12. H. Reichardt, "Vollständige darstellung der turbulenten geschwindigkeitsverteilung in glatten leitungen," *ZAMM - Zeitschrift für Angewandte Mathematik und Mechanik*, vol. 31, no. 7, pp. 208–219, 1951.

13. S. Hoyas and J. Jiménez, "Scaling of the velocity fluctuations in turbulent channels up to re=2003," *Physics of Fluids*, vol. 18, p. 011702, jan 2006.
14. J. Klinner, A. Hergt, S. Grund, and C. E. Willert, "High-speed PIV of shock boundary layer interactions in the transonic buffet flow of a compressor cascade," *Experiments in Fluids*, vol. 62, mar 2021.
15. D. Schlüß, C. Frey, and G. Ashcroft, "Consistent non-reflecting boundary conditions for both steady and unsteady flow simulations in turbomachinery applications," in *ECCOMAS Congress 2016 VII European Congress on Computational Methods in Applied Sciences and Engineering, Crete Island, Greece*, 2016.
16. P. Chandrashekar, "Kinetic energy preserving and entropy stable finite volume schemes for compressible euler and navier-stokes equations," *Communications in Computational Physics*, vol. 14, pp. 1252–1286, nov 2013.